Surgical and Radiologic Anatomy (2018) 40:587–597
https://doi.org/10.1007/s00276-018-2008-2

ORIGINAL ARTICLE

Three-dimensional computer-assisted dissection of pancreatic lymphatic anatomy on human fetuses: a step toward automatic image alignment

T. Bardol[1,2] · G. Subsol[3] · M.-J. Perez[4] · D. Genevieve[4,5,6] · A. Lamouroux[7] · B. Antoine[4] · G. Captier[8,9] · M. Prudhomme[1,2] · M. M. Bertrand[1,2]

Received: 2 September 2017 / Accepted: 20 February 2018 / Published online: 31 March 2018

Abstract

Purpose Pancreatic cancer is the fourth cause of death by cancer worldwide. Lymph node (LN) involvement is known to be the main prognostic factor. However, lymphatic anatomy is complex and only partially characterized. The aim of the study was to study the pancreatic lymphatic system using computer-assisted anatomic dissection (CAAD) technique and also to update CAAD technique by automatizing slice alignment.

Methods We dissected three human fetuses aged from 18 to 34 WA. 5-µm serial sections of duodeno-pancreas and spleen blocks were stained (hematoxylin–eosin, hematoxylin of Mayer and Masson trichrome), scanned, aligned and modeled in three dimensions.

Results We observed a rich, diffuse but not systematized lymphatic network in the peri-pancreatic region. There was an equal distribution of LNs between the cephalic and body–tail portions. The lymphatic vascularization appeared in continuity from the celiac trunk to the distal ends of its hepatic and splenic arterial branches parallel to the nerve ramifications of the celiac plexus. We also observed a continuity between the drainage of the pancreatic head and the para-aortic region posteriorly.

Conclusion In view of the wealth of peri-pancreatic LNs, the number of LNs to harvest could be increased to improve nodal staging and prognostic evaluation. Pancreatic anatomy as described does not seem to be compatible with the sentinel LN procedure in pancreatic surgery. Finally, we are now able to offer an alternative to manual alignment with a semi-automated alignment.

Keywords Pancreatic cancer · Lymphatic anatomy · Lymph node involvement · CAAD · Automatic image alignment

✉ T. Bardol
thomas.bardol@gmail.com

[1] Laboratory of Experimental Anatomy Faculty of Medicine Montpellier-Nimes, University Montpellier, 30 rue Lunaret, 34090 Montpellier, France

[2] Visceral and Digestive Surgery Department, CHU de Nimes, University Montpellier 1, Nîmes, France

[3] Research-Team ICAR, LIRMM CNRS, University of Montpellier, Montpellier, France

[4] Department of Medical Genetics, Reference Center for Developmental Abnormalities and Constitutional Bone Diseases, CHRU, Montpellier, France

[5] Genetics and Immunopathology of Inflammatory Osteoarticular Diseases, INSERM UMR1183, Montpellier, France

[6] University of Montpellier, Montpellier, France

[7] Obstetrics and Gynecology Department, Nîmes University Hospital, Nîmes, France

[8] Department of Plastic and Craniofacial Pediatric Surgery, Lapeyronie University Hospital, Avenue Du Doyen Gaston Giraud, Montpellier, France

[9] Epidemiological Biostatistics and Clinical Research Laboratory, EA2415, University of Montpellier, Montpellier, France

Introduction

Computer-assisted anatomic dissection (CAAD) was first described in the early 1990s and then improved in the 2010s [1, 30]. Since the first description, different anatomic studies have been done [1–3, 5–7, 17]. CAAD technique has allowed a precise anatomic description of the intra-pelvic innervation [1, 5, 17] that has led to new surgical approaches in pelvic surgery [6, 7]. This technique is accurate and inexpensive but very time-consuming as two major steps of this technique remain completely manual: alignment and segmentation. Most studies have been performed on human fetus specimens which provide some advantages such as a smaller sample, vascular anatomic structures (blood or lymph vessels) or nerves proportionally larger than in adult specimens. This time-consuming aspect has been a major drawback of this technique, limiting it to small sample anatomical studies, and is also a source of error and a lack of reproducibility.

Pancreatic cancer is one of the most lethal malignant pathologies in the world [34]. The main prognostic factor is lymph node (LN) involvement in the surgical specimen [10, 18, 25, 26]. Classically, LN involvement is caused by an invasion of the lymphatic vessels of the pancreatic gland, called node metastasis. However, lymphatic anatomy is still not fully understood and is extremely complex [8]. Currently, there is no reference to an anatomical nodal classification. French and international recommendations on LN dissection differ [20, 29]. The objective of this work was to precisely study the lymphatic drainage of the pancreas and look for the existence of a systematization of the lymphatic drainage. We also expected to improve the CAAD method by automating the alignment process.

Materials and methods

This study was carried out in the laboratory of experimental anatomy of the University of Montpellier–Nîmes and the Gynecology–Obstetric Department of the Montpellier University Hospital. This study was done in collaboration with the Informatics, Robotics and Micro-electronics Laboratory of Montpellier (LIRMM).

Specimens

We studied three human fetuses aged between 18 and 34 weeks of amenorrhea (Table 1). Fetuses were obtained from therapeutic abortion or late miscarriage, with donation of the fetus to research by the parents, as specified in French law. These procedures were performed at the Gynecology–Obstetric Department of the Montpellier University Hospital. The fetuses had no abnormalities in ante-natal ultrasound scan or macroscopical morphological abnormalities in the abdominal cavity and in particular in the duodeno-pancreas. The laboratory had the approval of the French Biological Agency. The laboratory of experimental anatomy of the University of Montpellier–Nimes had been integrated into the FETTAL, fetal enhanced three-dimensional and translational anatomical landscape, project (co-directed by Professors Genevieve and Captier) facilitating the acquisition of fetal tissues. Fetuses were collected with signed consent of the parents and in accordance with the French biomedical agency.

Macroscopical dissection

We removed "en bloc" for each fetus the duodeno-pancreas and the spleen. Samples were cut into 4-mm blocks then fixed at least 48 h in formalin (formaldehyde 10%). Then, the blocks were dehydrated and embedded in paraffin. We performed a series of 5-µm-thick transversal sections (from 3 to 5 sections) every 50 µm.

Histological study

Staining was done manually. Sections were stained with either hematoxylin–eosin (HE), hematoxylin of Mayer (HM) or Masson trichrome (Table 2).

HE or HM

The first section from each level was stained with HE or HM and used as the reference section.

Table 1 Characteristics of studied fetuses

Name	Gender	Term declared	FL (mm)	CRL (mm)	Estimated age (WA + days)	Cause of death	Delay to fixation (h)	Formalization	Fresh
01F-001	M	ND	38.3	270	22 + 2	ND	ND	15 years	−
17F-099	M	24 + 3	43.0	310	23 + 5	Myelomeningocele	88	48 h	+
17F-114	M	34	65.6	700	33 + 6	Achondroplasia	96	10 days	+

CRL crown-to-rump length, *FL* femur length, *WA* week of amenorrhea

Table 2 Histological characteristics of studied fetuses

Name	Section thickness (µm)	Spacement (µm)	Number of sections per level	Total number of sections	Staining	3D	Number of images treated for 3D
01F-001	5	50	3	547	HE and TM	Yes	290
17F-099	5	50	5	270	HM and TM	No	–
17F-114	5	50	5	350	HM and TM	No	–

3D three-dimensional reconstruction, *HE* hematoxylin–eosin, *HM* hematoxylin of Mayer, *TM* Masson trichrome

Masson trichrome

Masson trichrome was used to distinguish cells from the surrounding connective tissue.

Microscopic examination

We used a "Leitz Laborlux K" equipped with a digital camera "Canon EOS 400D DIGITAL". The optical enlargements available were ×4, ×10, ×25 and ×40. Analysis of the first section, stained by HE, made it possible to distinguish the different anatomical structures. Subsequent sections stained with Masson trichrome labeled collagen fibers of the fasciae in blue, allowing their relationship with the pancreatic gland to be ascertained. A lymphatic vascular element was identified upon presence of a single endothelium for any wall and the irregular distribution of the endothelial nuclei (valves were also observed by endothelium doubling). The difference between capillaries and lymphatic vessels, a larger channel following the capillaries, was related to the size of the lymphatic vasculature involved. The node mapping was performed by one person and then verified by an independent observer in order to prevent errors of interpretation. In case of disagreement on the localization of the LN, both observers studied the scanned version of the section together in order to find the right localization.

Three-dimensional reconstruction

The computer equipment used for acquisition and processing of images included: a MacBook Pro (Mac OS X Yosemite (version 10.10.5) plus Parallels Desktop version 5 software for Mac to install Windows 7 SP1); a high performance scanning system (EPSON Perfection V850 Pro); two image processing programs (Adobe Photoshop CC 2017 and ImageJ version 2.0.0); a WACOM Intuos Art Pen and Touch graphic tablet, for contouring of anatomical structures on digitized histological sections; and a 3D image reconstruction software (WinSurf, version 4.3).

All the sections were scanned using a high-resolution scanner (at 4800 dpi), aligned manually and then reconstructed in three dimensions. To do so, we manually contoured up to 16 anatomical structures (blood vessels, hollow and solid organs, LN) on each two-dimensional section using the graphic tablet. Each anatomical structure was then defined as a framework of points. The software WinSurf 4.3, via its "rendering engine", allowed conversion of the obtained points framework into polygons, to smooth out and to obtain a 3D projection of all the segmented elements [30].

Software and plug-ins (Table 3)

Fiji software was used to align sections [21]. We considered only free-access plug-ins because the LIRMM already used this software. We first analyzed four different programs pre-installed in the Fiji software in the "plug-ins". We excluded one (Template Matching and Slice Alignment) because it worked with gray-scale images, whereas our images were red–green–blue (RGB) colored. We thus tested three different plug-ins that worked with RGB images: StackReg [28], Register Virtual Stack Slices (RVSS) [4] and Linear Stack Alignment with SIFT (Scale Invariant Features Transform) [16].

Each plug-in had four different types of registration techniques of images: "translation", "rigid or rigid body" (translation + rotation), "similarity or scaled rotation" (translation + rotation + isotropic scale) and "affine" (free affine transformation). We excluded models of registration that did not respect the initial dimensions of the image ("similarity or scaled rotation" and "affine"). Therefore, we only tested "translation" and "rigid or rigid body" techniques of the plug-ins.

Table 3 Characteristics of the three different plug-ins tested

	Images/stack of images	Alignment method	Save as …
StackReg	Images	Sub-pixel based	JPEG
LSAS	Images	Feature-based	JPEG
RVSS	Stack	Feature-based	TIFF

LSAS Linear Stack Alignment with STIF, *RVSS* Register Virtual Stack Slices

Registration techniques

The purpose of registration was to align two or more different images into the same coordinate system. There were two types of registration techniques that used translation with or without rotation. Using an orthogonal scaling, translation authorized displacement of the image through x and y axis (Δx and Δy). Rotation of an angle σ was also permitted to align images. Thus, if we considered two images called $i1$ (reference image) and $i2$ (sensed image) while $i2'$ was the aligned version of $i2$, the aim of the registration was to determine Δx, Δy and σ so that $i1$ and $i2'$ were the most superimposable possible (Fig. 1). Thus, the goal of the registration was to obtain the shortest distance $d\,(i1; i2')$ possible. This distance, defined as the sum of the squared differences between the intensities, characterized the differences between two images.

We used two models of registration: feature-based and pixel/sub-pixel-based registrations as shown in Table 3. Initially, integral features of the image, such as corners, edges, contours or lines intersection, were used as control points (CPs) through their coordinates. Feature-based registration worked in four steps: feature detection, feature-matching, transform model estimation and image transformation [31]. The first step was to automatically detect CPs in the reference image while the second step was to identify similar CPs in the sensed image in order to process the registration (steps 3 and 4).

Pixel-based registration worked differently; this model mapped pixels in each image based on relative intensity patterns [11, 28]. The images were partitioned according to pixel-intensity and regrouped into clusters. Each cluster was represented by their coordinates. Sub-pixel is more accurate than pixel-based registration.

StackReg and Linear Stack Alignment with SIFT

StackReg and Linear Stack Alignment with SIFT (LSAS) worked with stacks of images. Both plug-ins worked similarly using the first image opened as a reference. After launching Fiji software, we loaded images using the "File" menu and the "Open" command (shortcut Cmd + O). Each image was loaded separately. We repeated this pattern as required. It was important to open images in a consecutive order. Secondly, we made a stack from the images opened using the "Images to Stack" command in "Stacks" section of the "Image" menu. Next we launched the plug-in through the "Plug-ins" menu and "Registration" section. When the alignment was complete, we used the command "Stack to Images" in "Stacks" section of the "Image" menu to acquire separate images from the stack as described above. We saved every image treated using the "Save As" command in the "File menu". Each picture was saved as a JPEG file.

Register Virtual Stack Slices

RVSS worked with separate images. The plug-in accepted all image types (8-bit, 16-bit, 32-bit and RGB), but only in .tif, .jpg, .png, .gif, .tiff, .jpeg, .bmp, .pgm or .ima format. The plug-in was launched through the "Plug-ins" menu, and an input folder with separate images was created. A reference image was selected and saved in the input folder to align each image. The aligned images were automatically saved as TIFF files in a chosen output folder.

Comparison

We chose the standard method of CAAD as a reference. The images were loaded, stacked and manually aligned using

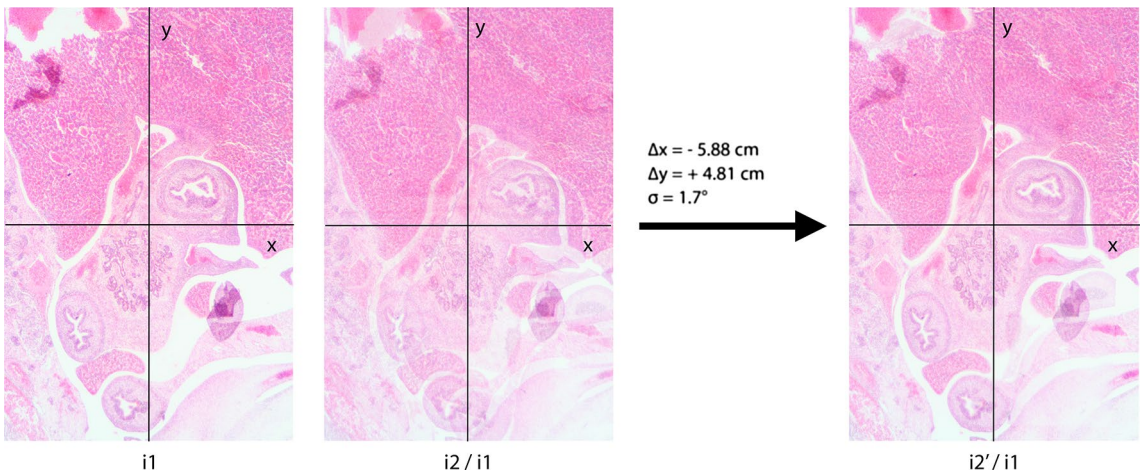

Fig. 1 Example of manual alignment of two different images of pancreatic buds from stage Carnegie 23 ($i1$ = referenced image; $i2$ = sensed image; $i2'$ = aligned version of i2)

the capacity of level transparency in Adobe Photoshop CC 2017. Then the same images were aligned using each plug-in. The results obtained by each plug-in were compared via two methods against the "manual alignment" version. First, two different people observed and compared manual and plug-ins alignment versions (qualitative comparison). Secondly, we compared the aligned stack of images obtained by measuring the distance between chosen landmarks (quantitative comparison). Finally, we compared each plug-in against the others.

Results

Pancreatic segmentation

Two-dimensional sections confirmed the anatomical descriptions as found in the anatomy and radiology atlases. The pancreas was described with a large oblique axis at the top, left and back. It consisted of three sectors:

- Right pancreas comprising the head embedded in the second part of the duodenum and limited forward by the gastro-duodenal artery as well as the uncus described behind the upper mesenteric vessels.
- Central pancreas comprising the pancreatic isthmus, forming the junction between the head and the body, behind which the portal vein was formed, delimited by two straight parallel lines, the first passing through the right edge of the upper mesenteric vein and the left border of the gastro-duodenal artery and the second by the left border of the superior mesenteric vein.
- Left pancreas comprising the body, oblique at the top, back and left, limited on the left at the intersection of the splenic artery pursued by the tail, the outermost parenchyma.

This three-part "anatomo-radiological" segmentation could also be supplemented by a three-part segmentation with a more "surgical" aim facilitating the analysis of LN distribution: the head, including uncinate process and neck; the body; and the tail.

Study of the pancreatic lymphatic network

Identification of peri-pancreatic node groups

Based on the three-part pancreatic segmentation, it was possible to detect five distinct peri-pancreatic LN groups (Fig. 2). We have not included celiac trunk or common hepatic artery LNs here. It was possible to demonstrate a few intra-parenchymal pancreatic LNs (Fig. 2b), mostly at the caudal portion of the pancreas but also at the level of the pancreatic head in the posterior part.

The cephalic LNs were equally distributed between the anterior and posterior surfaces of the head (Fig. 3; Table 4). The posterior cephalic LN group was partially represented by the lymphatic and node elements contained in the right retro-portal lamina. The LNs of the caudal group mainly came from the distal splenic artery.

We counted a total of 62 LNs distributed among the 5 groups for sample 01F-001 (Table 4).

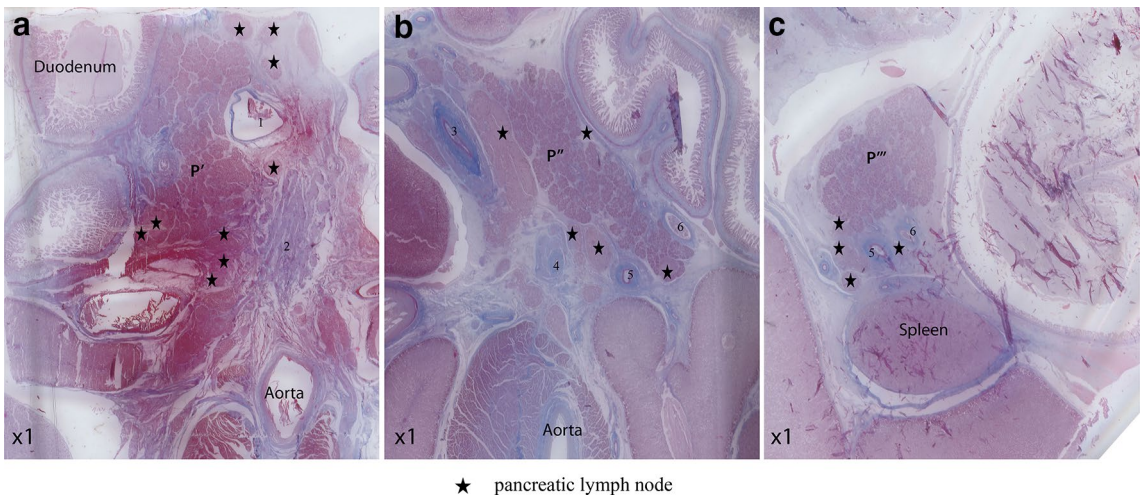

Fig. 2 Identification of distinct lymph node (LN) groups on Masson trichrome stained sections of fetal sample 01F-001: anterior and posterior cephalic LNs (**a**), anterior and posterior body LNs (**b**), caudal/splenic hilum LNs (**c**) (1: superior mesenteric vein, 2: superior mesenteric artery, 3: common hepatic artery, 4: left gastric artery, 5: splenic artery, 6: splenic vein, P′: pancreas head, P″: pancreas body, P‴: pancreas tail)

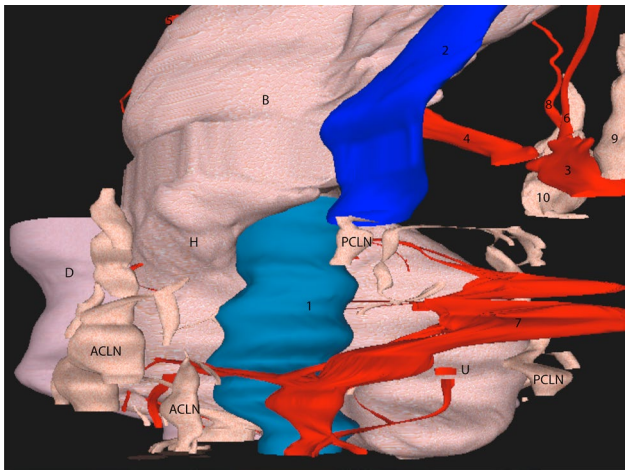

Fig. 3 Three-dimensional reconstruction of cephalic pancreatic lymph nodes (left lateral view) (*ACLN* anterior cephalic lymph nodes, *B* pancreatic body, *D* duodenum, *PCLN* posterior cephalic lymph nodes, *H* pancreatic head, *U* pancreatic uncus, 1: superior mesenteric vein, 2: splenic vein, 3: celiac trunk, 4: common hepatic artery, 5: gastro-duodenal artery, 6: splenic artery, 7: superior mesenteric artery, 8: left gastric artery, 9: left celiac ganglia, 10: right celiac ganglia)

For the second sample, 17F-099, we counted 31 cephalic LNs. It was not possible to estimate the number of body and tail nodes for this sample.

The third sample, 17F-114, showed a similar distribution to the first sample with a total of 69 nodes identified.

Nervous celiac plexuses and lymphatic drainage pathways

Through microscopic analysis of the sections, we observed the right and left celiac plexuses, as usually described, located behind and on either side of the celiac trunk. The celiac or semi-lunar nervous ganglia were thus distinguished: the left was oval, while the right one had a pyramidal shape (Fig. 4).

We observed that the lymphatic drainage was organized in parallel with the nerve fibers emanating from the celiac ganglia. Indeed, inside the plexuses, we visualized a significant concentration of capillaries and lymphatic vessels starting at the origin of the celiac trunk and continuing along the common hepatic artery (Figs. 5, 6). There was a continuity between the lymphatic vascularization of the base of the hepato-duodenal ligament and the origin of the celiac trunk throughout its circumference. A similar organization was observed enclosing the splenic artery (Fig. 7).

Improvement of the slice alignment

StackReg We started the test with all images of interest loaded and stacked as explained above. When we ran the plug-in, the random access memory (RAM) needed to execute was too high causing a systems crash. Thus, we limited the test to stacks of only 15 consecutive images.

Regardless of the technique used ("translation" or "rigid body"), the alignment was quite rapid (around a minute per aligned image). However, we faced the same problem for both registration techniques. When the images were similar and "easily aligned manually", the alignment was efficient. But if there were a major difference between two consecutive sections, the images were progressively deviated laterally which led to a high loss of image content. This phenomenon was even worse for translation associated with rotation transformation compared to translation alone.

Register Virtual Stack Slices As explained above, this plug-in worked with an input file containing the images of interest. We initiated the tests using the file containing all images. We faced a different problem to the one encountered with the first plug-in. When the images were too dissimilar (for example image number 001 and number 056), the alignment terminated because the plug-in did not recognize enough reference landmarks between the images. We therefore decided to use files containing only 15 consecutive images as before.

"Translation" technique gave better results than with StackReg plug-in, but sometimes the alignment lacked accuracy. Due to the absence of "rotation" transformation, alignment was not good enough.

"Rigid" technique was efficient and the alignment was accurate. This plug-in was faster than StackReg (about

Table 4 Anatomic repartition in five groups of the peri-pancreatic lymph nodes identified on fetal samples

Localization	01F-001		17F-099		17F-114	
	Number	Ratio (%)	Number	Ratio (%)	Number	Ratio (%)
Anterior cephalic	22	35.5	19	61.3	21	30.4
Posterior cephalic	11	17.7	12	38.7	12	17.4
Anterior body	2	3.2	ND	ND	9	13
Posterior body	15	24.2	ND	ND	16	23.2
Tail/splenic hilum	12	19.4	ND	ND	11	16
	62	100	31	100	69	100

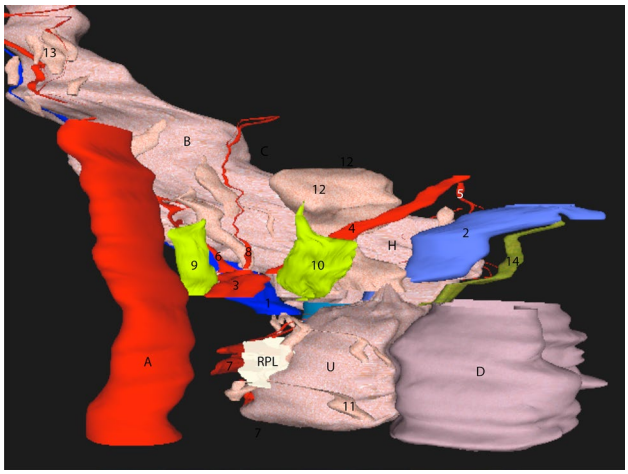

Fig. 4 Three-dimensional reconstruction of nervous celiac ganglions (posterior view) (*A* aorta, *B* pancreatic body, *D* duodenum, *H* pancreatic head, *RPL* right retro-portal lamina, *U* pancreatic uncus, 1: splenic vein, 2: portal vein, 3: celiac trunk, 4: common hepatic artery, 5: gastro-duodenal artery, 6: splenic artery, 7: superior mesenteric artery, 8: left gastric artery, 9: left celiac ganglia, 10: right celiac ganglia, 11: posterior cephalic LN, 12: posterior body LN, 13: tail LN, 14: common bile duct)

30–45 s per image treated) regardless of the technique chosen. For both techniques, the program modified dimensions of the canvas to avoid loss of content of the images.

Linear Stack Alignment with SIFT We began the test with a stack containing all the images. Alignment failed because the maximum memory limit was reached. Consequently, we used stacks of 15 consecutive images. The plug-in was extremely fast (less than 10 s per image). As expected, alignment was better when using "rigid" technique than "translation". We improved the results by increasing the maximum alignment error (which was the maximal allowed transfer error of a match to be counted as a good one) to 50 pixels. However, we observed a significant loss of image content because the plug-in did not enlarge canvas size.

Comparison In comparison with the standard manual alignment technique, StackReg gave the worst results due to deteriorated images. It was also the least accurate of the tested plug-ins (Table 5). From our experience, this program was not adapted to improve CAAD technique. In contrast (Table 5), RVSS and LSAS obtained comparable results in terms of accuracy and were both faster than manual alignment (approximately 2 times faster for RVSS and 5 times faster for LSAS). LSAS allowed accurate registration but also image content loss. Moreover, the plug-in was not easy to use. In contrast, RVSS was very simple to handle and did not deteriorate images thanks to its ability to enlarge image canvas without modifying its content. Thus, RVSS appeared to be the best plug-in (Table 5) and also a good alternative to manual alignment (Table 6).

Discussion

This study investigated three key anatomical areas where LNs are concentrated: the pancreatic head, the pancreas body and the splenic hilum. Our morphological study of the pancreas allowed us to observe that peri-pancreatic LNs are numerous and almost equally divided between the cephalic and body–tail parts in the peri-pancreatic region. We described lymphatic pathways forming a parallel network to the nerve ramifications of the celiac plexus extending from the origin of the celiac trunk to the distal ends of its hepatic and splenic arterial branches. From our experience, RVSS appears to be the best plug-in to improve CAAD technique.

A minimum number of 15 LNs should be harvested in pancreatic surgery for curative purposes according to a US cohort study [22]. In another study, Vuarnesson et al. demonstrated that a minimum number of 16 LNs should be taken during pancreatico-duodenectomy to obtain a reliable assessment of *N* status [33]. Moreover, it has been shown that risk of under-staging is inversely proportional to the number of LNs removed [13, 14, 24, 32]. More recently, a Canadian study [23], comparing the 1990–2000 and

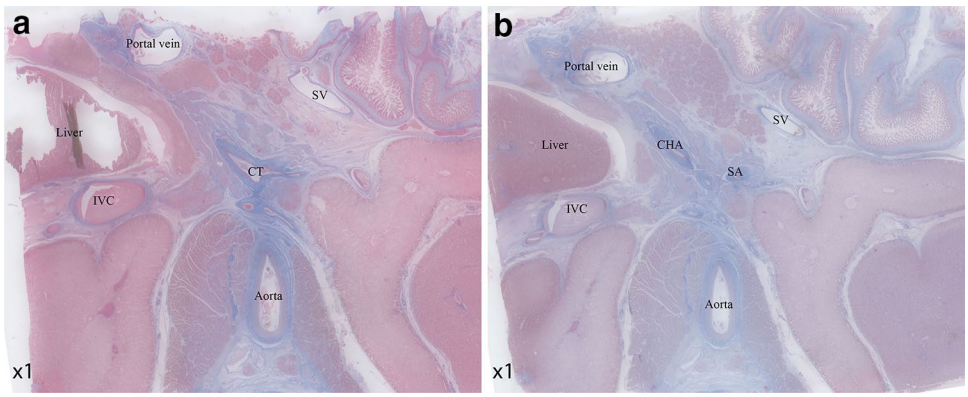

Fig. 5 Masson trichrome-stained sections from fetal sample 01F-001 showing nervous and lymphatic elements in continuity from the origin of the celiac trunk at 360° to the common hepatic artery: origin of CT (**a**) and proximal CHA and proximal SA (**b**) (*CHA* common hepatic artery, *CT* celiac trunk, *IVC* inferior vena cava, *SA* splenic artery, *SV* splenic vein)

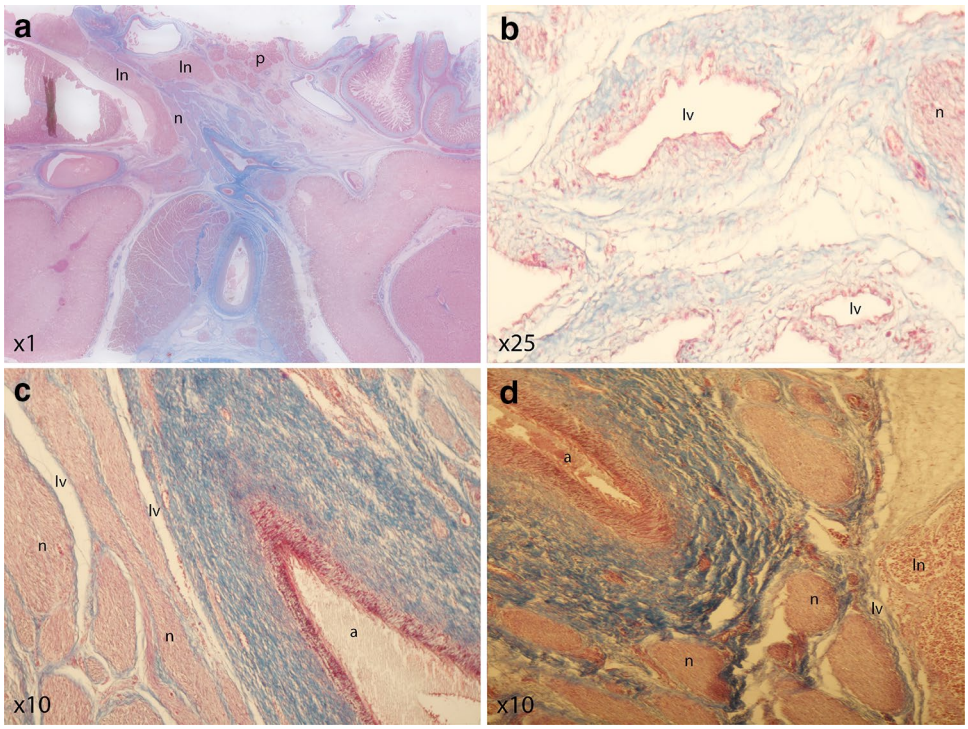

Fig. 6 Lymphatic vessels under light microscope at different magnifications on Masson trichrome-stained sections of fetal sample 01F-001. **a** Section showing the celiac trunk (CT); **b** irregular-walled lymphatic vessels at the origin of the CT; **c** lymph vessels at the origin of the common hepatic artery (CHA) surrounded by nerve fibers emanating from a nerve plexus; **d** nerve fibers and lymph vessels running along the CHA (*a* common hepatic artery, *ln* lymph node, *lv* lymph vessel, *n* nerve fiber, *p* pancreas)

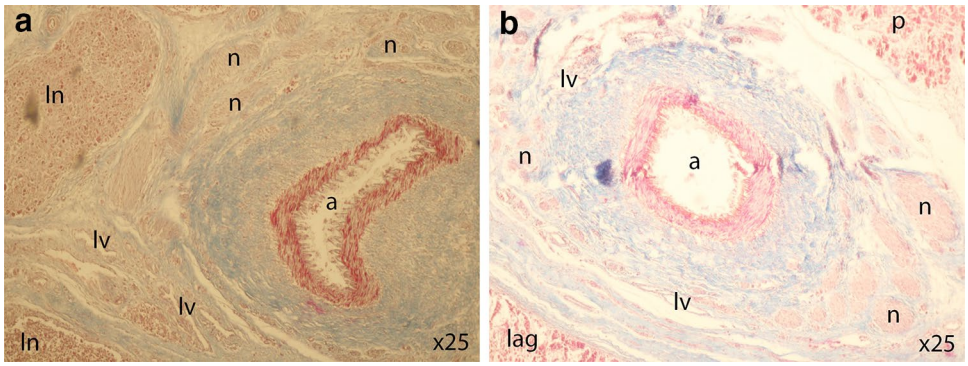

Fig. 7 Presence of lymphatic vascular elements surrounding the splenic artery on Masson trichrome-stained sections of fetal sample 01F-001: proximal splenic artery (**a**), distal portion of the splenic artery (**b**) (*a* splenic artery, *lag* left adrenal gland, *ln* lymph node, *lv* lymph vessel, *n* nerve fiber, *p* pancreas)

Table 5 Comparative table of the three plug-ins tested

	Best model of registration	Accuracy	Time spent (s/image)	Major drawback
StackReg	Translation	++[a]/−−−[b]	60	Loss of image content
RVSS	Rigid	+++	30–45	None
LSAS	Rigid	++	10	Loss of image content

RVSS Register Virtual Stack Slices, *LSAS* Linear Stack Alignment with SIFT

[a]If images were really similar

[b]If images were too much different

2000–2010 periods, showed that the median number of LNs removed increased significantly (7 vs. 17) as well as the percentage of *N*+ patients (58 vs. 69%) over time. The main consequence of this evolution was the significant increase in the use of adjuvant therapies: 30% in 1990–2000 and 63% in 2000–2010 leading to an improvement of the median of survival [23]. Thus, the minimum number of 12 LNs to harvest, according to the ISGPS recommendations, may appear low. It could easily be increased to at least 16 for any pancreatic oncological surgery, as proposed by Vuarnesson et al. for Whipple procedures [33] in order to improve the *N*-staging.

Our results concerning the different drainage pathways are consistent with the findings of Hirono et al. [12] who

Table 6 Comparison between Register Virtual Stack Slices and manual alignment

	Model of registration	Alignment method	Accuracy	Time-consuming
Manual alignment	Translation and rotation	Manual	+	+++
RVSS	Rigid	Feature-based	+++	+

RVSS Register Virtual Stack Slices

demonstrated the existence of seven drainage channels at the head of the pancreas, including the anterior and posterior pancreatico-duodenal arches, the hepato-duodenal ligament or the para-aortic region. However, the lymphatic arborescence did not seem to correspond to the concept of sentinel LN. For example, a study concluded that it was impossible to perform the sentinel LN procedure in the case of adenocarcinoma of the pancreas [15]. Furthermore, the issue of LN harvesting from targeted LN stations (common hepatic artery LN/HALN or para-aortic LN/PALN) remains open.

CAAD is a precise technique that has proven benefits in surgery. However, its major drawback is the time needed to align sections that has limited a wider use of the technique. In our study, we benefited from LIRMM's experience in terms of treatment of medical imaging [19, 27]. To begin with, regardless of the plug-in used it was not possible to treat all images simultaneously. It appeared mandatory to treat series of images and we chose to treat 15 image stacks. However, this gave us two advantages. First, limiting the number of consecutive images of interest reduced the risk of treating too many different images and therefore the risk of alignment errors. The second was that the smaller sample size resulted in faster alignment. The lack of processing alignment was due to the capacity of the computer we used for the study. Indeed, the software was unable to process the registration because the RAM needed was insufficient. Thus, this could be easily corrected using a much more powerful processor. Of the three plug-ins tested, the one that gave the best results was RVSS. We obtained very satisfying results in terms of alignment using "Rigid" transformation. Also, RVSS was the only one that had the capacity to enlarge canvas size in order to prevent loss of image content. Moreover, this enlargement had no impact on the image size itself. RVSS was also faster than manual alignment and very easy to use. Whilst the time gained was not as great as anticipated (we included the time needed to open images, launch the plug-in and save the aligned images), the partial automation of the stack alignment left the observer free to complete other tasks.

However, this study has some limitations. First, we only studied three fetuses. We were also not able to successfully perform immuno-labeling of the lymph vessels using anti-LYVE antibody, because our samples were fixed in formalin at least 72 h after therapeutic abortion. The samples were not fresh enough to obtain positive immuno-labeling results. However, standard staining such as hematoxylin–eosin or Masson trichrome are reliable to identify LNs via microscopic examination of each section. Indeed using these stains, we precisely identify the LN capsule and germinal centers inside LN. This node mapping step was verified by an independent person (Bertrand MM) who also examined each section to look for interpretation errors. In all cases the concordance between observers was perfect. Whilst hematoxylin–eosin or Masson trichrome staining are less accurate than immuno-labeling to identify the lymph vessels, this double examination reduced interpretation errors and made the node mapping reproducible for this study.

Concerning, the improvement of alignment method, we decided to test strictly free-access software which limited the number of plug-ins of interest. We could have used "Reconstruct" software [9] which is also free, or used landmarks included inside paraffin blocks as "control points" to improve our alignment method. We chose Fiji because the LIRMM had extensive experience with this software. Finally, we used a free software because our laboratory could not afford to buy multiple expensive software. Finally, WinSurf, version 4.3 was easy to use but presented some drawbacks. First, the contouring of anatomical structures was entirely manual and was time-consuming. Secondly, an offset of a few microns between successive sections was almost imperceptible when we focus only on these two sections but at the scale of stack of images it was responsible for either a unilateral continuous shift called "Tower of Pisa" effect or a zig-zag effect. In the first case, this shift was often highlighted at the time of segmentation and disrupted the entire alignment. In the second case (zig-zag effect), it was possible to smooth this effect using the "Smooth object" option but the results were not as accurate due to content loss.

Conclusion

To conclude, we observed a diffuse but non-systematized lymphatic vascularization in the peri-pancreatic region. Quantitatively, there is an even LN distribution between the cephalic and body–tail portions. Compared to the nodal peripancreatic wealth, the number of nodes to harvest could be increased to improve nodal staging and prognostic evaluation. Lymphatic vascularization appears in continuity from the celiac trunk to the distal ends of its hepatic and splenic arterial branches parallel to the nerve ramifications of the celiac plexus. We have also observed a continuity between

the drainage of the pancreatic head and the para-aortic region behind. This anatomy does not seem to be compatible with the performance of the sentinel LN procedure in pancreatic surgery.

We did not find the perfect plug-in that could process all the images simultaneously, and make an accurate alignment without deteriorating the images. However, although we have failed to achieve a fully automatic alignment procedure, we are able to offer an alternative to manual alignment. This option is accurate, does not deteriorate the content of images and takes much less time. Thus, RVSS represents a step towards full automatic image alignment by providing a semi-automated alignment.

Acknowledgements Thanks to the University of Montpellier that awarded us a grant to perform this study and to Sarah Kabani for English language assistance.

Compliance with ethical standards

Conflict of interest The authors declare that they have no conflicts of interest.

References

1. Alsaid B, Bessede T, Diallo D, Karam I, Uhl JF, Delmas V, Droupy S, Benoît G (2012) Computer-assisted anatomic dissection (CAAD): evolution, methodology and application in intrapelvic innervation study. Surg Radiol Anat 34:721–729
2. Alsaid B, Bessede T, Karam I, Abd Alsamad I, Uhl JF, Benoît G, Droupy S, Delmas V (2009) Coexistence of adrenergic and cholinergic nerves in the inferior hypogastric plexus: anatomical and immunohistochemical study with 3D reconstruction in human male fetus. J Anat 214:645–654
3. Alsaid B, Moszkowicz D, Peschaud F, Bessede T, Zaitouna M, Karam I, Droupy S, Benoit G (2011) Autonomic-somatic communications in the human pelvis: computer-assisted anatomic dissection in male and female fetuses. J Anat 219:565–573
4. Arganda-Carreras I, Sorzano CO, Marabini R, Carazo JM, Ortiz-de-Solorzano C, Kybic J (2006) Consistent and elastic registration of histological sections using vector-spline regularization. In: International workshop on computer vision approaches to medical image analysis. Springer, Berlin, pp 85–95
5. Bertrand M, Alsaid B, Droupy S, Benoit G, Prudhomme M (2014) Biomechanical origin of the Denonvilliers' fascia. Surg Radiol Anat 36:71–78
6. Bertrand M, Alsaid B, Droupy S, Benoit G, Prudhomme M (2013) Optimal plane for nerve sparing total mesorectal excision, immunohistological study and 3D reconstruction: an embryological study. Colorectal Dis 15:1521–1528
7. Bertrand M, Colombo P, Alsaid B, Prudhomme M, Rouanet P (2014) Transanal endoscopic proctectomy and nerve injury risk: bottom to top surgical anatomy, key points. Dis Colon Rectum 57:1145–1148
8. Cesmebasi A, Malefant J, Patel SD, Plessis MD, Renna S, Tubbs RS, Loukas M (2015) The surgical anatomy of the lymphatic system of the pancreas. Clin Anat 28:527–537
9. Fiala JC (2005) Reconstruct: a free editor for serial section microscopy. J Microsc 218:52–61
10. Fujita T, Nakagohri T, Gotohda N, Takahashi S, Konishi M, Kojima M, Kinoshita T (2010) Evaluation of the prognostic factors and significance of lymph node status in invasive ductal carcinoma of the body or tail of the pancreas. Pancreas 39:e48–e54
11. Gerogiannis D, Nikou C, Likas A (2007) Rigid image registration based on pixel grouping. In: Image analysis and processing, 2007. ICIAP 2007. 14th international conference on, 2007. IEEE, pp 595–602
12. Hirono S, Tani M, Kawai M, Okada K-i, Miyazawa M, Shimizu A, Uchiyama K, Yamaue H (2012) Identification of the lymphatic drainage pathways from the pancreatic head guided by indocyanine green fluorescence imaging during pancreaticoduodenectomy. Dig Surg 29:132–139
13. House MG, Gönen M, Jarnagin WR, D'Angelica M, DeMatteo RP, Fong Y, Brennan MF, Allen PJ (2007) Prognostic significance of pathologic nodal status in patients with resected pancreatic cancer. J Gastrointest Surg 11:1549–1555
14. Huebner M, Kendrick M, Reid-Lombardo KM, Que F, Therneau T, Qin R, Donohue J, Nagorney D, Farnell M, Sarr M (2012) Number of lymph nodes evaluated: prognostic value in pancreatic adenocarcinoma. J Gastrointest Surg 16:920–926
15. Kocher H, Sohail M, Benjamin I, Patel A (2007) Technical limitations of lymph node mapping in pancreatic cancer. Eur J Surg Oncol 33:887–891
16. Lowe DG (2004) Distinctive image features from scale-invariant keypoints. Int J Comput Vis 60:91–110
17. Moszkowicz D, Alsaid B, Bessede T, Penna C, Benoit G, Peschaud F (2011) Female pelvic autonomic neuroanatomy based on conventional macroscopic and computer-assisted anatomic dissections. Surg Radiol Anat 33:397–404
18. Murakami Y, Uemura K, Sudo T, Hayashidani Y, Hashimoto Y, Nakashima A, Yuasa Y, Kondo N, Ohge H, Sueda T (2010) Number of metastatic lymph nodes, but not lymph node ratio, is an independent prognostic factor after resection of pancreatic carcinoma. J Am Coll Surg 211:196–204
19. Ourselin S, Roche A, Subsol G, Pennec X, Ayache N (2001) Reconstructing a 3D structure from serial histological sections. Image Vis Comput 19:25–31
20. Sauvanet A (2008) Lymph node resection for carcinoma of the pancreas. J de chirurgie 145:12S31-12S35
21. Schindelin J, Arganda-Carreras I, Frise E, Kaynig V, Longair M, Pietzsch T, Preibisch S, Rueden C, Saalfeld S, Schmid B (2012) Fiji: an open-source platform for biological-image analysis. Nat Methods 9:676–682
22. Schwarz RE, Smith DD (2006) Extent of lymph node retrieval and pancreatic cancer survival: information from a large US population database. Ann Surg Oncol 13:1189–1200
23. Serrano PE, Cleary SP, Dhani N, Kim PT, Greig PD, Leung K, Moulton C-A, Gallinger S, Wei AC (2015) Improved long-term outcomes after resection of pancreatic adenocarcinoma: a comparison between two time periods. Ann Surg Oncol 22:1160–1167
24. Slidell MB, Chang DC, Cameron JL, Wolfgang C, Herman JM, Schulick RD, Choti MA, Pawlik TM (2008) Impact of total lymph node count and lymph node ratio on staging and survival after pancreatectomy for pancreatic adenocarcinoma: a large, population-based analysis. Ann Surg Oncol 15:165
25. Sohn TA, Yeo CJ, Cameron JL, Koniaris L, Kaushal S, Abrams RA, Sauter PK, Coleman J, Hruban RH, Lillemoe KD (2000) Resected adenocarcinoma of the pancreas—616 patients: results, outcomes, and prognostic indicators. J Gastrointest Surg 4:567–579
26. Strobel O, Hinz U, Gluth A, Hank T, Hackert T, Bergmann F, Werner J, Büchler MW (2015) Pancreatic adenocarcinoma: number of positive nodes allows to distinguish several *N* categories. Ann Surg 261:961–969

27. Subsol G, Thirion J-P, Ayache N (1998) A scheme for automatically building three-dimensional morphometric anatomical atlases: application to a skull atlas. Med Image Anal 2:37–60
28. Thevenaz P, Ruttimann UE, Unser M (1998) A pyramid approach to subpixel registration based on intensity. IEEE Trans Image Process 7:27–41
29. Tol JA, Gouma DJ, Bassi C, Dervenis C, Montorsi M, Adham M, Andrén-Sandberg A, Asbun HJ, Bockhorn M, Büchler MW (2014) Definition of a standard lymphadenectomy in surgery for pancreatic ductal adenocarcinoma: a consensus statement by the International Study Group on Pancreatic Surgery (ISGPS). Surgery 156:591–600
30. Uhl J-F, Hammoudi SS, Delmas V (2015) Un nouvel outil de recherche en morphologie: la dissection anatomique assistée par ordinateur (DAAO). Morphologie 99:112
31. Vaghasiya PP, Gautam PK (2015) Image registration techniques: a review. Int J Eng Comput Sci 4:10489–10492
32. Valsangkar NP, Bush DM, Michaelson JS, Ferrone CR, Wargo JA, Lillemoe KD, Fernández-del Castillo C, Warshaw AL, Thayer SP (2013) N0/N1, PNL, or LNR? The effect of lymph node number on accurate survival prediction in pancreatic ductal adenocarcinoma. J Gastrointest Surg 17:257–266
33. Vuarnesson H, Lupinacci R, Semoun O, Svrcek M, Julié C, Balladur P, Penna C, Bachet J, Resche-Rigon M, Paye F (2013) Number of examined lymph nodes and nodal status assessment in pancreaticoduodenectomy for pancreatic adenocarcinoma. Eur J Surg Oncol 39:1116–1121
34. Zhang Q, Zeng L, Chen Y, Lian G, Qian C, Chen S, Li J, Huang K (2016) Pancreatic cancer epidemiology, detection, and management. Gastroenterol Res Pract 2016:8962321